

# Comparative study of gel-based separated arc-discharge, HiPCO, and CoMoCAT carbon nanotubes for macroelectronic applications

Jialu Zhang<sup>§,1</sup>, Hui Gui<sup>§,2</sup>, Bilu Liu<sup>1</sup>, Jia Liu<sup>3</sup>, and Chongwu Zhou<sup>1</sup> (✉)

*Nano Res.*, **Just Accepted Manuscript** • DOI: 10.1007/s12274-013-0368-9  
<http://www.thenanoresearch.com> on September 7 2013

© Tsinghua University Press 2013

## Just Accepted

This is a “Just Accepted” manuscript, which has been examined by the peer-review process and has been accepted for publication. A “Just Accepted” manuscript is published online shortly after its acceptance, which is prior to technical editing and formatting and author proofing. Tsinghua University Press (TUP) provides “Just Accepted” as an optional and free service which allows authors to make their results available to the research community as soon as possible after acceptance. After a manuscript has been technically edited and formatted, it will be removed from the “Just Accepted” Web site and published as an ASAP article. Please note that technical editing may introduce minor changes to the manuscript text and/or graphics which may affect the content, and all legal disclaimers that apply to the journal pertain. In no event shall TUP be held responsible for errors or consequences arising from the use of any information contained in these “Just Accepted” manuscripts. To cite this manuscript please use its Digital Object Identifier (DOI®), which is identical for all formats of publication.

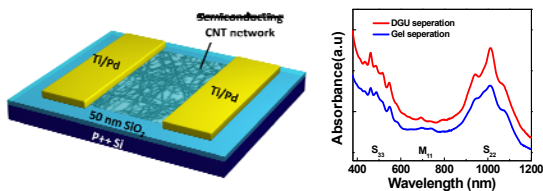
## TABLE OF CONTENTS (TOC)

### Comparative Study of Gel-based Separated Arc-discharge, HiPCO, and CoMoCAT Carbon Nanotubes for Macroelectronics Applications

Jialu Zhang<sup>§1</sup>, Hui Gui<sup>§2</sup>, Bilu Liu<sup>1</sup>, Jia Liu<sup>3</sup> and Chongwu Zhou<sup>\*</sup>

University of Southern California, USA

Page Numbers. The font is ArialMT 16 (automatically inserted by the publisher)



# Comparative Study of Gel-based Separated Arc-discharge, HiPCO, and CoMoCAT Carbon Nanotubes for Macroelectronic Applications

Jialu Zhang<sup>§1</sup>, Hui Gui<sup>§2</sup>, Bilu Liu<sup>1</sup>, Jia Liu<sup>3</sup> and Chongwu Zhou<sup>1</sup>(✉)

<sup>1</sup> Department of Electrical Engineering, University of Southern California, Los Angeles, California 90089, USA.

<sup>2</sup> Department of Chemical Engineering and Material Science, University of Southern California, Los Angeles, California 90089, USA.

<sup>3</sup> Department of Chemistry, University of Southern California, Los Angeles, California 90089, USA.

<sup>§</sup> These authors contributed equally to this work.

Received: day month year / Revised: day month year / Accepted: day month year (automatically inserted by the publisher)

© Tsinghua University Press and Springer-Verlag Berlin Heidelberg 2011

## ABSTRACT

Due to their excellent electrical property and compatibility with room-temperature deposition/printing processing, high-purity single-walled semiconducting carbon nanotubes hold great potential for macroelectronic application such as thin-film transistors and display back-panel electronics. However, the relative advantages and disadvantages of various nanotubes for macroelectronics remains an open issue, despite the great significance. Here in this paper, we report comparative and systematic study of three kinds of mainstream carbon nanotubes (arc-discharge, HiPCO, CoMoCAT) separated using low-cost gel-based column chromatography for thin-film transistor applications, and high performance transistors, which satisfy the requirement of transistors used in active matrix organic light-emitting diode displays, have been achieved. We observe a trade-off between transistor mobility and on/off ratio depending on the nanotube diameter. While arc-discharge nanotubes with larger diameters lead to high device mobility, HiPCO and CoMoCAT nanotubes with smaller diameters can provide high on/off ratio ( $>10^6$ ) for transistors with comparable dimensions. Furthermore, we have also compared gel-based separated nanotubes with nanotubes separated using density gradient ultracentrifuge (DGU) method, and find that gel-separated nanotubes can offer purity and thin-film transistor performance as good as DGU-separated nanotubes. Our approach can serve as the critical foundation for future carbon nanotube-based thin-film macroelectronics.

## KEYWORDS

Separated carbon nanotubes, thin-film transistors, gel-based column chromatography, purity of semiconducting nanotubes, diameter-dependence

## Introduction

Since first discovered in 1991[1], carbon nanotubes (CNT) have attracted a lot of attention due to their extraordinary electrical properties such as high intrinsic carrier mobility and current-carrying capacity[2-4]. While significant progress has been made toward making nanoscale transistors based on individual or aligned CNTs for nanoelectronics[5-12], we reported in 2009 that thin-films of separated carbon nanotubes can work as the channel material for thin-film transistors (TFT) used in display back-panel electronics[13]. Other popular TFT channel materials, such as amorphous silicon[14] and organic materials[15-17] suffer from their low carrier mobility, while polycrystalline silicon[18,19] and metal oxide[20,21] typically require high-cost and high-temperature processing. Compared with all the materials above, nanotube thin-films have the advantages of low-cost room-temperature processing, superb transparency, excellent flexibility, high device performance, and compatibility with printing technologies. During the past four years, inspired by density-gradient ultracentrifuge (DGU) carbon nanotube separation method developed by Hersam and his coworkers[22,23], high-performance TFTs using pre-separated semiconducting nanotubes have been fabricated by us and several other groups [13,24,25]. In those previous reports, transistors exhibit high on/off ratio ( $>10^5$ ) as well as excellent current drive capability ( $\sim 1 \mu\text{A}/\mu\text{m}$ ), and applications such as digital logic circuits[26,27], transparent electronics[28] and active matrix organic light-emitting diode (AMOLED) displays[29] have been demonstrated. Recently, several groups [30,31] have reported a gel-based column chromatographic nanotube separation method, which is very simple and inexpensive. By this method, high-purity semiconducting and even single chirality

nanotubes[32,33] can be separated, and devices fabricated using gel-based separated nanotubes show excellent electrical performance[34]. Due to these merits, gel-based separated semiconducting nanotubes look very promising for TFT applications such as display electronics. In spite of the significant progress reported so far, many interesting issues remain to be studied. For example, among all the mainstream nanotubes, which kind of nanotubes is most suitable for TFT applications? Is the nanotube diameter a key factor affecting the gel-based separated nanotube thin-film transistor (SN-TFT) performance? What are the requirements for TFTs used in AMOLED displays? Are gel-based SN-TFTs good enough for AMOLED display applications? Do gel-based separated nanotubes have electrical properties as good as DGU-based separated nanotubes?

To answer the above-mentioned questions, we report our recent advance on comparative and systematic study of three kinds of mainstream carbon nanotubes separated using low-cost gel-based column chromatography for macroelectronics applications. Our work includes the following essential components. (1) We carried out gel-based column chromatography for arc-discharge nanotubes (Carbon Solutions, Inc), HiPCO nanotubes (Unidym, Inc), and CoMoCAT nanotubes (Sigma Aldrich, Inc). High-purity semiconducting nanotubes were achieved. (2) SN-TFTs were fabricated using the three kinds of gel-based separated nanotubes, and key device performance metrics such as on-current density, on/off ratio, sheet resistance and device mobility are directly compared. Based on the detailed analysis, we have revealed a trade-off between transistor mobility and on/off ratio depending on the nanotube diameter, and find that arc discharge nanotubes with larger diameters

offer high mobility, while HiPCO and CoMoCAT nanotubes with small diameters can provide high on/off ratio. (3) In addition, we have also compared the electrical properties of gel-based and DGU-based semiconducting nanotubes, and similar electrical performance was observed for both kinds of semiconducting nanotubes. Our gel-based SN-TFT platform shows significant advantages over conventional platforms with respect to cost, scalability, reproducibility, and device performance, and suggests a practical and realistic approach for nanotube-based AMOLED display applications.

## Results and discussion

To carry out nanotube separation, all three kinds of nanotubes were first dispersed in aqueous solution. Arc-discharge nanotubes were dispersed in water with the assistance of sodium cholate (SC, Sigma-Aldrich (99%)) at a concentration of 1 mg/mL, while HiPCO and CoMoCAT nanotubes were dispersed in aqueous solution assisted by 1% sodium dodecyl sulfate (SDS, Sigma-Aldrich (99%)) at 0.3 mg/ml and 1 mg/mL, respectively. Following that, ultra-sonication and centrifugation were applied to these CNT suspensions to remove bundles and impurities. Then, all three kinds of nanotubes went through gel-based separation process. Specifically, sephacryl medium (GE healthcare, Inc) was used to fill the column for succeeding nanotube separation. More details about nanotube dispersion and gel-based column chromatography can be found in the "Method" section.

After nanotube separation, we have characterized gel-based column chromatographic separated nanotubes. Three kinds of carbon nanotubes, namely arc-discharge nanotubes, HiPCO nanotubes, and CoMoCAT nanotubes were selected and studied in this work. These three kinds of nanotubes have similar defect ratios (Fig. S-1 in the Electronic Supporting Material

(EMS)) but very distinct diameter distribution. Arc-discharge nanotubes have diameters about 1.3 nm to 1.7 nm, which is larger than HiPCO nanotubes (0.8 nm to 1 nm) and CoMoCAT nanotubes (~ 0.7 nm). Due to this diameter difference, different optical and electrical properties were observed for these three kinds of separated nanotubes, which will be discussed later in this article.

Figure 1 shows the comparison of gel-based column chromatographic separated arc-discharge, HiPCO and CoMoCAT nanotubes. The optical absorption spectra before (blue) and after (red) gel-based separation are plotted in Figure 1a-c (a: arc-discharge nanotubes; b: HiPCO nanotubes; c: CoMoCAT nanotubes). Based on these curves, one can estimate the purity of the separated semiconducting nanotubes, which is 98%, 92% and 95%, respectively. The purity of separated semiconducting nanotubes is calculated using the optical absorption spectroscopy evaluation [35], which is well accepted by researchers in the carbon nanotube field. This estimation method typically has an error around a few percent. In this regard, the purities we have obtained each with one round of gel chromatography separation (98% for arc-discharge, 92% for HiPCO, 95% for CoMoCAT) are within the error margin of the absorption spectroscopy evaluation. The diameter information can also be extracted, where arc-discharge semiconducting nanotubes exhibit a diameter range of 1.3 nm to 1.7 nm, while HiPCO and CoMoCAT nanotubes show diameter range of 0.8 nm to 1 nm and ~ 0.7 nm, respectively. Because of their different diameter distribution, these three kinds of separated nanotubes exhibit different optical properties, which can be seen from the peak positions in the optical absorption spectra, as well as the color of the separated semiconducting nanotube solutions shown in the insets of Figure 1a-c (light brown for arc-discharge semiconducting nanotubes; dark green for HiPCO semiconducting

nanotubes; purple for CoMoCAT semiconducting nanotubes). Detailed calculation of the purity and diameter information can be found in ESM Fig. S-2.

Other than purity and diameter, nanotube length also plays a crucial role for nanotube thin-film transistor performance.

To characterize the length distribution of the three kinds of gel-based separated semiconducting nanotubes, more than one hundred tubes from each kind were imaged and measured by field-emission scanning electron microscopy (FE-SEM), and the

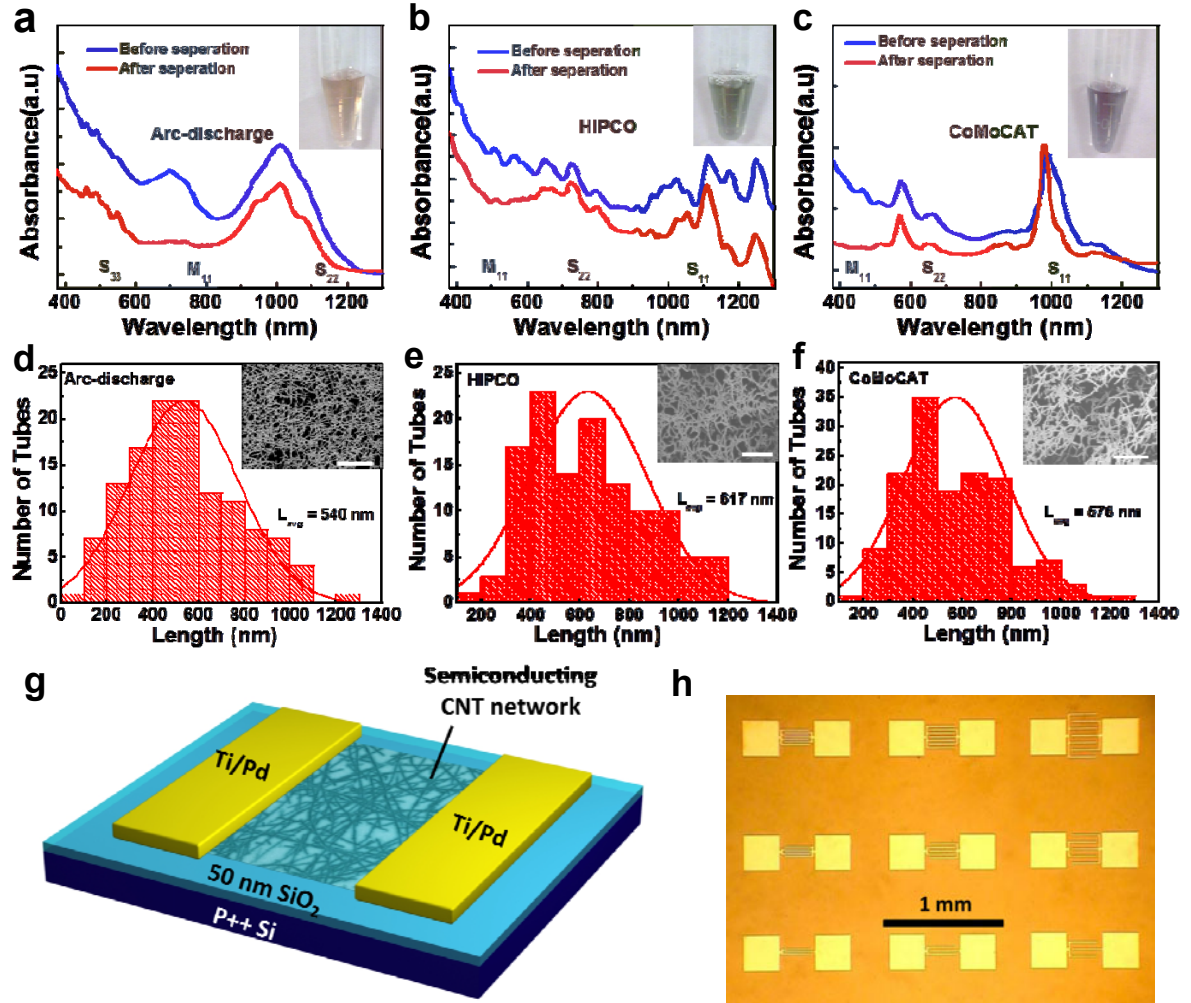


Figure 1. Comparison of gel-based column chromatographic separated nanotubes synthesized by different methods. (a-c) Optical absorption spectra of arc-discharge nanotubes (a), HiPCO nanotubes (b), and CoMoCAT nanotubes (c) before (blue) and after (red) separation. Inset: Nanotube solutions after separation. (d-f) Length distribution of the separated semiconducting arc-discharge nanotubes (d), HiPCO nanotubes (e), and CoMoCAT nanotubes (f), the average nanotube length is 540 nm, 617 nm, and 576 nm, respectively. Inset: FE-SEM images of separated semiconducting nanotubes network deposited on Si/SiO<sub>2</sub> substrates with APTES functionalization, where the scale bar is 1  $\mu$ m. (g) Schematic diagram of a back-gated SN-TFT. (h) Optical microscope image of the SN-TFT array fabricated on silicon substrate with 50 nm SiO<sub>2</sub> acting as gate dielectric.



histograms are shown in Figure 1 d-f. From these plots, one can find that arc-discharge nanotubes, HiPCO nanotubes, and CoMoCAT nanotubes show similar average nanotube lengths, which are 540 nm, 617 nm and 576 nm, respectively. This similarity of nanotube length distribution is due to the fact that similar nanotube dispersion recipe was applied for all three kinds of nanotubes, which can also be found in the Methods Section. As all these three kinds of separated nanotubes are similar in terms of semiconducting purity and nanotube length, they can be the ideal materials to study the effect of diameter on the electrical performance of SN-TFTs.

To fabricate SN-TFT devices, high density, uniform separated nanotube thin films were deposited on Si/SiO<sub>2</sub> substrates using the solution-based aminosilane-assisted separated nanotube deposition technique reported in our previous publications [13]. FE-SEM is used to inspect the samples after nanotube assembly and the SEM images of the arc-discharge, HiPCO, and CoMoCAT semiconducting nanotubes deposited on Si/SiO<sub>2</sub> substrates are shown in the inset of Figure 1d-f, respectively. The nanotube deposition recipes were carefully adjusted so as all. These three kinds of nanotubes have similar area nanotube density, which is measured to be 32-41 tubes/ $\mu\text{m}^2$  for arc-discharge nanotubes, 27-38 tubes/ $\mu\text{m}^2$  for HiPCO nanotubes, and 26-36 tubes/ $\mu\text{m}^2$  for CoMoCAT nanotubes. After nanotube assembly, the deposited separated nanotube thin films were used for back-gated SN-TFTs fabrication (see Methods). The schematic diagram of the back-gated SN-TFTs and the optical microscope image of a fabricated SN-TFT array are shown in Figure 1g and h, respectively.

Electrical performance of gel-separated arc-discharge, HiPCO and CoMoCAT TFTs is compared and exhibited in Figure 2. Such SN-TFTs are made with channel width ( $W$ ) of 200, 400, 800, 1200, 1600, and 2000  $\mu\text{m}$ , and channel length ( $L$ ) of 4, 10, 20, 50, and

100  $\mu\text{m}$ . Based on these devices, we have carried out systematic measurement and analysis of the electrical performance of the SN-TFTs. Figure 2a-c are the normalized transfer characteristics ( $I_D/W-V_G$ ) of the SN-TFTs using arc-discharge (Figure 2a), HiPCO (Figure 2b) and CoMoCAT (Figure 2c) semiconducting nanotubes with various channel lengths (4, 10, 20, 50, and 100  $\mu\text{m}$ ) and fixed channel width (2000  $\mu\text{m}$ ) plotted in logarithm scale. All the curves were measured at  $V_D = 1\text{V}$ . From the figures, the following behaviors can be observed. (1) Devices from all nanotube samples show p-type field-effect behavior and very high on/off ratios. (2) As the device channel length increases, the on/off ratio increases while the on-current decreases. In addition, all three kinds of devices exhibit on/off ratio higher than  $10^6$  when the channel length is longer than 50  $\mu\text{m}$ . (3) The devices using arc-discharge semiconducting nanotubes with larger diameters exhibit better on-current but lower on/off ratio than HiPCO and CoMoCAT semiconducting nanotubes which have relatively smaller diameters.

Figure 2d-f exhibit the transfer characteristics (red: linear scale, green: log scale) and  $g_m-V_G$  characteristics (blue) of typical SN-TFTs using three kinds semiconducting nanotubes measured at  $V_D = 1\text{V}$ . All the devices have a channel length of 10  $\mu\text{m}$  and width of 2000  $\mu\text{m}$ . Based on these plots, one can find the key device performance metrics of these three devices. For the arc-discharge SN-TFT (Figure 2d), the on-current density ( $I_{on}/W$ ) at  $V_D = 1\text{V}$  and  $V_G = -10\text{V}$  is measured to be 0.34  $\mu\text{A}/\mu\text{m}$ , and on/off ratio is  $2 \times 10^4$ . The transconductance ( $g_m$ ) can also be extracted from the maximum slope of the transfer characteristics, which is 113  $\mu\text{S}$ . For the HiPCO SN-TFT (Figure 2e), on-current density is 0.066  $\mu\text{A}/\mu\text{m}$ , on/off ratio is  $3.6 \times 10^6$ , and transconductance is 33  $\mu\text{S}$ . For CoMoCAT SN-TFT (Figure 2f), the on-current density, on/off ratio, and transconductance are calculated to be

0.0175  $\mu\text{A}/\mu\text{m}$ ,  $1.6 \times 10^7$ , and 10.6  $\mu\text{S}$ , respectively. The corresponding output characteristics ( $I_D$ - $V_D$ ) of these three SN-TFTs are also plotted in Figure 2g-i, respectively. Under small  $V_D$  biases, the devices exhibit linear behavior, indicating that ohmic contacts are formed between the metal electrodes and the nanotubes. Saturation behaviour was observed when

more negative  $V_D$  was applied, indicating nice field-effect operation.

As mentioned previously, the separated arc-discharge, HiPCO, and CoMoCAT nanotubes have distinctively different diameters, but are similar in length and network density. To get a more comprehensive understanding of the diameter dependent electrical performance

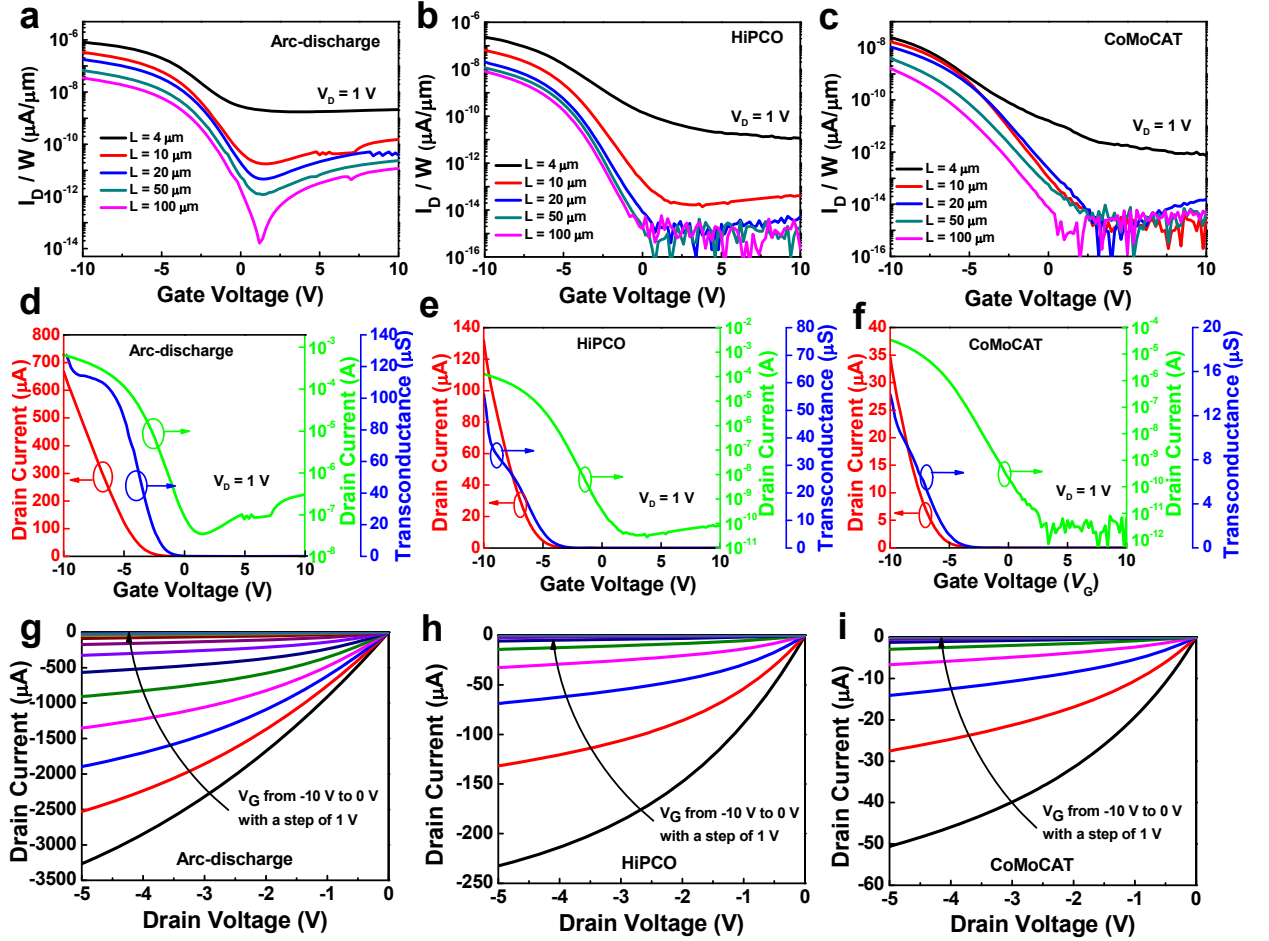


Figure 2. Electrical properties of back-gated SN-TFTs using gel-based separated semiconducting nanotubes synthesized with different methods. (a-c) Normalized transfer characteristics ( $I_D/W$ - $V_G$ ) of the SN-TFTs using semiconducting arc-discharge nanotubes (a), HiPCO nanotubes (b), and CoMoCAT nanotubes (c) with various channel lengths (4, 10, 20, 50, and 100  $\mu\text{m}$ ) and 2000  $\mu\text{m}$  channel width plotted in logarithm scale. (d-f) Transfer characteristics (red: linear scale, green: log scale) and  $g_m$ - $V_G$  characteristics (blue) of a typical SN-TFT ( $L = 10 \mu\text{m}$ ,  $W = 2000 \mu\text{m}$ ) using semiconducting arc-discharge nanotubes (d), HiPCO nanotubes (e), and CoMoCAT nanotubes (f). (g-i) Output characteristics ( $I_D$ - $V_D$ ) of the same devices in (d-f).

behaviour, we have compared the key device performance metrics such as on-current density, channel sheet resistance, on/off ratio, and device mobility for SN-

TFTs based on those three kinds of gel-based separated semiconducting nanotubes. Figure 3 summarizes the results after the measurement of 180 SN-TFTs with different



semiconducting nanotube diameters, and various channel lengths and channel widths. Figure 3a shows the normalized on-current densities ( $I_{on}/W$ ) of the transistors with various channel lengths measured at  $V_D = 1$  V and  $V_G = -10$  V, showing that the on-current density is approximately inversely proportional to the channel length for all three kinds of semiconducting nanotubes. The highest on-current density is measured to be  $1 \mu A/\mu m$ , which comes from SN-TFTs using separated arc-discharge semiconducting nanotubes with a channel length of  $4 \mu m$ . Overall, with the same device dimension, SN-TFTs using arc-discharge nanotubes provides about 5 times higher on-current density than the ones using HiPCO nanotubes, and about 17 times higher on-current density than the ones with CoMoCAT nanotubes. This conclusion is also consistent with the data shown in Figure 2.

To understand the reason of this on-current density difference, we have analysed the contact resistivity and channel sheet resistance of these three different kinds of devices using transfer length method (TLM). For each transistor, we know that the total device resistance ( $R_{tot}$ ) equals to the sum of the contact resistance ( $R_c$ ) and channel resistance ( $R_{ch}$ ). As  $R_{ch} = R_{\square}L/W$ , where  $R_{\square}$  is the sheet resistance of the separated nanotube film, the total resistance can be described as:  $R_{tot} = R_c + R_{\square}L/W$  or  $R_{tot}W = R_cW + R_{\square}L$ . It means that at fixed channel width, the scaled device resistance ( $R_{tot}W$ ) follows a linear relationship with the channel length, while the slope stands for the sheet resistance ( $R_{\square}$ ) and the intercept stands for the scaled contact resistance ( $R_cW$ ). Therefore, using the scaled device resistance data obtained at gate bias of  $-10$  V with different channel length, we can derive the scaled contact resistance and channel sheet resistance of the three different kinds of SN-TFTs, and the results are plotted in Figure 3b. From this figure, one can find that the contact resistances for SN-TFTs are negligible

compared with channel sheet resistance. And the calculated channel sheet resistances for arc-discharge SN-TFTs, HiPCO SN-TFTs, and CoMoCAT SN-TFTs are  $0.28 M\Omega/\square$ ,  $1.10 M\Omega/\square$  and  $6.52 M\Omega/\square$ , respectively. As the sheet resistance is dominated by the tube-to-tube junction resistance [36], we can conclude that large-diameter nanotubes provide smaller junction resistance than small-diameter nanotubes. One contributing factor can be that large-diameter nanotubes have larger tube-to-tube contact area, and therefore smaller junction resistance. Other factors may include how holes transport from one nanotube to another, which needs further study for a thorough understanding. Overall, we find that SN-TFTs using large-diameter nanotubes are superior to the ones using small-diameter nanotubes in terms of channel sheet resistance, which is also the reason why higher on-current density is observed for devices fabricated with larger-diameter nanotubes. As noted before, the purities of our three kinds of nanotubes are with the error margin of each other using the absorption spectroscopy evaluation. In addition, the metallic nanotube density is way below the percolation threshold to form a conductive path from source to drain, and we therefore believe the difference in on-current density above mentioned mainly comes from the semiconducting nanotube networks.

Besides on-current density, the other important device parameter is current on/off ratio, which is calculated as the current at  $V_G = -10$  V divided by the minimum current measured for  $V_D = 1$  V, and the results are plotted in Figure 3c. From this plot, one can find that as the channel length increases, the average on/off ratio of all three kinds of SN-TFTs increases, which is due to the decrease in the probability of percolative transport through metallic nanotubes as the device channel length increases. It is worth noting that for HiPCO and CoMoCAT SN-TFTs, we observe that the average on/off ratio

decreases slightly when the channel length is longer than 50  $\mu\text{m}$ . This is because although both the on-current and off-current should decrease when the channel length increases, when the channel length is

sufficiently long, the off-current would reach the noise level of the measurement equipment (Agilent 4156 B Semiconducting Parameter Analyzer with an accuracy of 1 pA), and then would not decrease further.

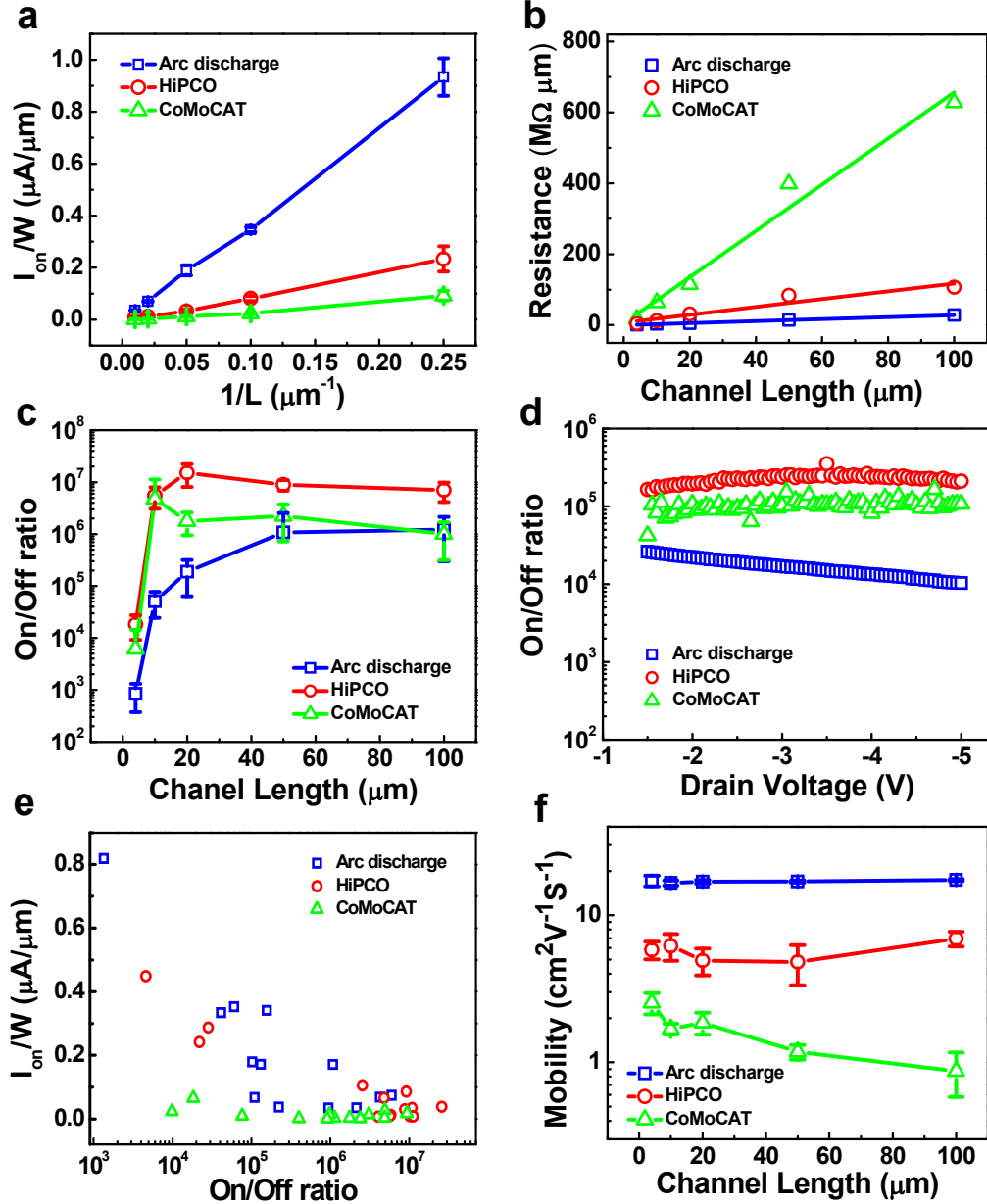


Figure 3. Statistical study and key device performance metrics comparison of SN-TFTs using separated nanotubes with different synthetic methods. (a) Current density ( $I_{\text{on}}/W$ ) versus reversed channel length for TFTs fabricated on separated semiconducting nanotubes synthesized by arc-discharge (blue), HiPCO (red), and CoMoCAT (green) methods. Plot of (b) device resistance and (c) average on/off ratio ( $I_{\text{on}}/I_{\text{off}}$ ) versus channel length for the same TFTs characterized in (a). (d) Trade-off between Current density ( $I_{\text{on}}/W$ ) and on/off ratio ( $I_{\text{on}}/I_{\text{off}}$ ). (e) On/off ratio ( $I_{\text{on}}/I_{\text{off}}$ ) versus drain voltage for devices using three different kinds of semiconducting nanotubes with  $L = 50 \mu\text{m}$  and  $W = 1200 \mu\text{m}$ . (f) Relationship between device mobility and channel length for three kinds of SN-TFTs.

Therefore, we observed a slightly decrease of the on/off ratio for long channel devices.

In addition, from Figure 3c, we also observe that under the same channel length, the on/off ratios of arc-discharge SN-TFTs is lower than the on/off ratios of HiPCO and CoMoCAT SN-TFTs, which means large-diameter SN-TFTs have higher off-current than small-diameter SN-TFTs. There are two possible sources for the off-current, which are the percolative transport through metallic nanotubes and the thermal excitation of carriers through semiconducting nanotubes [37]. For short channel devices, the former source is believed to be the main reason of the off-current because the channel length is comparable to the length of nanotubes. On the other hand, when the channel length is much longer than nanotube length, based on the 2D stick model[38], the percolation threshold density ( $N$ ) can be expressed as the following equation:

$$N = \frac{1}{\pi} \left( \frac{4.236}{l} \right)^2$$

where  $l$  is the average length of the nanotubes. If we take arc-discharge nanotubes as an example ( $l = 540$  nm),  $N$  can be calculated to be 20 tubes/  $\mu\text{m}^2$ . As only about 2% of the separated arc-discharge nanotubes are metallic, in order to form a metallic pathway for the long channel devices, the totally nanotube density needs to reach 1000 tubes/  $\mu\text{m}^2$ , which is much higher than the real nanotube density we measured (32-41 tubes/ $\mu\text{m}^2$ ). Therefore, the percolative transport through metallic nanotubes is negligible for long channel devices, which suggests that the off-current mainly comes from the thermal excitation of carriers. As we know, the bandgap ( $E_g$ ) of a nanotube is reversely proportional to the diameter ( $d$ ) of the nanotube, which can be written as  $E_g = 2\gamma_0 a_{c-c}/d$ , where  $\gamma_0$  is the C-C tight-binding overlap energy, and  $a_{c-c}$  is the nearest-neighbour C-C distance (0.142 nm). Based on literature,  $\gamma_0$  is around 2.7 eV[3,4], so we can derive that the bandgap ranges for arc-

discharge nanotubes, HiPCO nanotubes and CoMoCAT nanotubes are 0.45-0.59 eV, 0.77-0.95 eV, and 1.09 eV, respectively. Thermal excitation can be strongly suppressed for small-diameter separated nanotube TFTs because of their large bandgap. However, for large-diameter nanotubes (arc-discharge nanotubes), due to their small bandgap, non-negligible amount of thermally excited carriers can be present in the semiconducting nanotubes and flow through the channel to form a non-negligible off-current, which leads to lower on/off ratio than small-diameter nanotube devices (HiPCO and CoMoCAT SN-TFTs). It is worth noting that due to the noise limit of the equipment mentioned above and the high device resistance for CoMoCAT nanotube thin films, CoMoCAT SN-TFTs exhibit lower on/off ratio than HiPCO SN-TFTs when the channel lengths are long. However, the off-current of CoMoCAT SN-TFTs is actually lower than HiPCO SN-TFTs before it reaches the noise level, which is shown in Fig. S-3 in the ESM.

The conclusion above is further supported by the results shown in Figure 3d, where typical devices using three kinds of nanotubes with the same channel dimension ( $L = 50$   $\mu\text{m}$ ,  $W = 1200$   $\mu\text{m}$ ) were characterized. This plot shows us the on/off ratio of the arc-discharge SN-TFTs decreases when the source-to-drain voltage increases, while the on/off ratios for HiPCO and CoMoCAT SN-TFTs remain the same under different drain biases. The decrease of the on/off ratio for arc-discharge SN-TFTs is attributed to the fact that carriers will gain more energy under a high source-to-drain bias, and therefore, more carriers will be able to transport through the channel due to thermal excitation, which will result in a higher off-current and a lower on/off ratio. In contrary, the wide bandgap of HiPCO and CoMoCAT semiconducting nanotubes can effectively suppress the thermal excitation even under a high source-to-drain voltage, and thus a nearly constant on/off ratio is observed.

This phenomenon further proves that instead of percolative transport through metallic nanotubes, thermal excitation of carriers is the main source of the off-current for long channel SN-TFTs. This diameter-dependent on/off ratio behaviour also suggests that small-diameter nanotubes are preferred for applications which need high biases and high on/off ratios.

Interestingly, the data shown in Figure 3a and 3c also reveal a trade-off between drive-current and on/off ratio, both of which are key parameters for display applications. On one hand, larger-diameter nanotubes and shorter channel length can help to achieve higher on-current density due to the small sheet resistance. On the other hand, the narrow bandgap associated with large diameter nanotubes will give rise to more thermal excitation, and shorter channel length can also increase the possibility of percolative transport through metallic nanotubes, thus leading to higher off-current and lower on/off ratio. The plot in Figure 3e clearly illustrates this trade-off. One of the most promising applications of carbon nanotube thin-film transistors is AMOLED display electronics, where current drive capability and on/off ratio are the most crucial merits. Unlike liquid crystal display (LCD), where voltage-controlled circuit is applied, current-controlled circuit is required for AMOLED displays, which means the current flow through the driving transistors will directly go through the OLED pixels, and therefore, decide the output light intensity of the OLED. Due to this reason, high current drive capability is required for TFTs used in AMOLED displays to create enough light intensity within a certain area. For 40-inch high-definition television (HDTV), in order to reach a brightness of 600 Cd/m<sup>2</sup>, about 12  $\mu\text{A}$  current needs to be delivered to a pixel with an area of 153×460  $\mu\text{m}^2$  [39], which means that, if two-transistor control circuit is applied in each pixel, a minimum unit areal current drive of 0.00034  $\mu\text{A}/\mu\text{m}^2$  needs to be satisfied for the driving

transistors in the circuitry. Besides driving current, on/off ratio is another crucial parameter for display electronics. As progressive scanning is used in most of the display circuits nowadays, each pixel will only be programmed for a very short time during one frame time. In order to have a smooth picture, the switching transistors of each display pixel need to have high enough on/off ratio to hold the light intensity constant. The larger the display, the higher on/off ratio is needed, and based on literature [40], on/off ratio needs to reach 10<sup>6</sup> for 256 grayscale 1080P displays. From Figure 3e, we can find that for the three kinds of SN-TFTs, if on/off ratio of 10<sup>6</sup> is required, the highest measured on-current density for arc-discharge SN-TFTs is 0.17  $\mu\text{A}/\mu\text{m}$ , which comes from a device with a channel length of 20  $\mu\text{m}$ , while the highest on-current density for HiPCO and CoMoCAT SN-TFTs is 0.11  $\mu\text{A}/\mu\text{m}$  ( $L = 10 \mu\text{m}$ ) and 0.014  $\mu\text{A}/\mu\text{m}$  ( $L = 10 \mu\text{m}$ ), respectively. In addition, if we calculate the maximum on-current drive per unit area, the value can be derived to be 0.0085  $\mu\text{A}/\mu\text{m}^2$  for arc-discharge SN-TFTs, 0.011  $\mu\text{A}/\mu\text{m}^2$  for HiPCO SN-TFTs, and 0.0014  $\mu\text{A}/\mu\text{m}^2$  for CoMoCAT SN-TFTs. One interesting finding is that although under the same channel geometry, arc-discharge SN-TFTs exhibit about 5 times higher on-current density than HiPCO SN-TFTs, these two kinds of SN-TFTs provide similar maximum on-current drive per unit area for devices with an on/off ratio higher than 10<sup>6</sup>, which is due to the trade-off between on-current density and device on/off ratio. Overall, based on our analysis, all three kinds of SN-TFTs meet the basic requirements for transistors used in AMOLED displays.

Besides the on-current density and on/off ratio, we have also characterized device mobility ( $\mu_{\text{device}}$ ) for all three kinds of SN-TFTs. Device mobility of the SN-TFTs is extracted following the equation:

$$\mu_{\text{device}} = \frac{L}{V_D C_{\text{ox}} W} \cdot \frac{dI_d}{dV_g} = \frac{L}{V_D C_{\text{ox}}} \cdot \frac{g_m}{W},$$

where  $L$  and  $W$  are the device channel length and width,  $V_D = 1$  V, and  $C_{ox}$  is the gate capacitance per unit area. Here, we use the following equation[41,42]:

$$C_{ox} = \left\{ C_{\varphi}^{-1} + \frac{1}{2\pi\epsilon_0\epsilon_{ox}} \ln \left[ \left( \frac{\Lambda_0}{R} \frac{\sinh(2\pi t_{ox} / \Lambda_0)}{\pi} \right) \right] \right\}^{-1} \Lambda_0^{-1}$$

to calculate the gate capacitance as it considers the electrostatic coupling of nanotubes.  $\Lambda_0^{-1}$  stands for the density of nanotubes and is measured to be around 10 tubes/ $\mu\text{m}$ ,  $C_0 = 4.0 \times 10^{-10}$  F/m is the quantum capacitance of nanotubes[43]. And  $\epsilon_0\epsilon_{ox} = 3.9 \times 8.85 \times 10^{-14}$  F/cm is the gate dielectric constant. The device mobility of three kinds of SN-TFTs is plotted in Figure 3f. Among these three kinds of SN-TFTs, arc-discharge SN-TFTs give the highest mobility, which is around 17  $\text{cm}^2/\text{Vs}$ . HiPCO and CoMoCAT SN-TFTs show mobility around 5  $\text{cm}^2/\text{Vs}$  and 1  $\text{cm}^2/\text{Vs}$ , respectively. These data illustrates that large-diameter SN-TFTs provide higher mobility than small-diameter SN-TFTs, which is consistent with the device sheet resistance analysis discussed above. We noted that the mobility around 17  $\text{cm}^2/\text{Vs}$  we report here for separated arc discharge tubes is lower than the mobility of around 30  $\text{cm}^2/\text{Vs}$  we reported previously[26]. One reason is that we used relatively low nanotube density ( $\sim 32\text{--}41$  tubes/ $\mu\text{m}^2$ ) to achieve high on/off ratio (e.g.  $>10^6$  for  $L \geq 50\mu\text{m}$ ), while the previous study[26] used 41 tubes/ $\mu\text{m}^2$  to achieve higher mobility at the cost of lower on/off ratio ( $\sim 10^5$ ). Other factors affecting the mobility include batch-to-batch variation of nanotube quality, variation in nanotube surfactants and length as well as different gate dielectric structures[25].

One important issue we want to point out is that although mobility is the key metric for other thin-film transistor channel materials, it is not the best parameter to evaluate the performance of carbon nanotube TFTs. The reason is that mobility can only directly reflect the current drive capability, but cannot reveal the on/off ratio

information of the given transistors. It may not be a problem for other TFT channel materials, such as amorphous silicon, polycrystalline silicon, or metal oxide, because all those materials have constant on/off ratio regardless of the channel geometry once their doping level or element composition is fixed. However, due to the existence of metallic nanotube, carbon nanotubes TFTs exhibit a trade-off between on-current density and on/off ratio depending on the transistor geometry. Therefore, it is not fair to evaluate the performance of nanotube TFTs by just comparing the mobility, which cannot account for the on/off ratio difference between different transistors. One good example is the comparison between arc-discharge and HiPCO SN-TFTs we discussed above. Although arc-discharge SN-TFTs show about three times higher mobility than HiPCO SN-TFTs, these two kinds of devices exhibit similar on-current drive when the device on/off ratio is required to be higher than  $10^6$ . For this reason, we think for carbon nanotube TFTs, it is better to compare the maximum current drive capability under certain on/off ratio requirement rather than compare the device mobility alone.

Based on the analysis above, we have found that different separated semiconducting nanotubes exhibit different electrical properties. Table 1 summarizes all the differences we have discussed so far for arc-discharge, HiPCO and CoMoCAT separated nanotubes, including semiconducting nanotube purity, nanotube diameter, electrical bandgap, maximum on-current density for devices with on/off ratio higher than  $10^6$ , device mobility, and channel sheet resistance. Overall, we find that large diameter nanotubes provide smaller sheet resistance, higher transconductance, and higher device mobility. Hence, large-diameter nanotubes have advantage in applications which require high carrier mobility, such as radio frequency circuits. In contrary, small-

diameter nanotubes show higher on/off ratio and smaller off-current, which may be preferred for digital circuit applications, where on/off ratio and power consumption are big concerns. Also, we can conclude that all three kinds of separated nanotubes satisfy the general requirement of AMOLED display applications, which demand certain current drive and high on/off ratio.

Table 1.

	Arc-discharge	HiPCO	CoMoC AT
Purity	98%	92%	95%
Diameter (nm)	1.3-1.7	0.8-1	~0.7
Energy band(eV)	0.45-0.59	0.77-0.95	~1.09
On-current density when on/off ratio >10 <sup>6</sup> ( $\mu\text{A}/\mu\text{m}$ )	0.17	0.11	0.014
Device Mobility ( $\text{cm}^2\text{V}^{-1}\text{S}^{-1}$ )	8.8 $\pm$ 0.27	3.0 $\pm$ 0.62	0.78 $\pm$ 0.067
Sheet resistance ( $\text{M}\Omega/\square$ )	0.28	1.10	6.52

Our ability to fabricate high performance gel-based SN-TFTs enabled us to further explore their application in display electronics. For the proof of concept purpose, an organic light-emitting diode (OLED) was connected to and controlled by a typical HiPCO SN-TFT device whose transfer characteristic is shown in Figure S4a in the ESM. In order to control OLED, device on-current and on/off ratio are crucial. Here the device channel length and channel width are selected to be 20  $\mu\text{m}$  and 1200  $\mu\text{m}$  so that the transistor can provide enough current while the on/off reaches 10<sup>6</sup> and therefore can meet the requirement for controlling the OLED to switch on and off. Standard NPD/Alq<sub>3</sub> OLED (2  $\times$  2 mm<sup>2</sup>) with multi-layered configuration is employed in this study given as ITO/4-4'-bis[N-(1-naphthyl)-N-phenyl-amino]bi-phenyl (NPD) [40 nm]/tris(8-hydroxyquinoline) aluminium (Alq<sub>3</sub>) [40 nm]/LiF [1 nm]/aluminium (Al) [100 nm], whose transfer characteristics are shown in the Figure S4b in the ESM. The schematic of the OLED control circuit is shown in the inset

of Figure 4a, where the drain of the driving transistor was connected to an external OLED and a negative voltage ( $V_{\text{DD}}$ ) was applied to the cathode of the OLED. Current flow through OLED ( $I_{\text{OLED}}$ ) can be modified by varying the voltage applied to  $V_{\text{G}}$ , as directly revealed in Figure 5a where current *versus*  $V_{\text{G}}$  characteristics are plotted with a fixed  $V_{\text{DD}}$  of -8 V. From this figure and the inset optical photographs taken at certain gate voltages, one can find that the light intensity of the OLED is modulated by the gate voltage and it can be fully turned on and turned off when  $V_{\text{G}}$  are biased at -10 V and 10 V, respectively. Furthermore, current flow through the OLED was also measured by sweeping the  $V_{\text{DD}}$  while also changing the input voltage  $V_{\text{G}}$  as plotted in Figure 4b. The figure illustrates that the tested OLED has a threshold voltage of about 3 V and it will be turned on when the controlling transistor is in the “ON” state and the supply voltage is higher than the OLED threshold voltage.

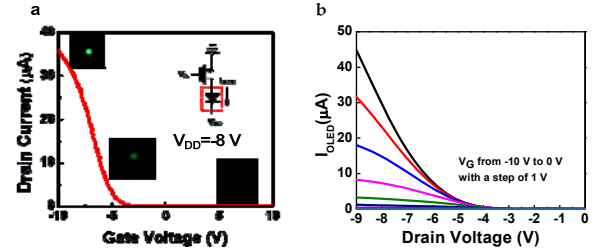


Figure 4. External OLED controlled by HiPCO SN-TFTs. (a) Plot of the current through the OLED ( $I_{\text{OLED}}$ ) versus  $V_{\text{G}}$  with  $V_{\text{DD}} = -8 \text{ V}$ . The inset optical images show the OLED intensity at certain gate voltages. And the inset schematic image is the diagram of the OLED control circuit. (b)  $I_{\text{OLED}}-V_{\text{DD}}$  Characteristics of the OLED control circuit. Various curves correspond to various values of  $V_{\text{G}}$  from -10 to 0 V in 1 V steps.

In addition to the electrical performance comparison between different kinds of gel-based separated semiconducting nanotubes,



we are also very interested in the device performance comparison between SN-TFTs using nanotubes separated by gel-based column chromatography and nanotubes separated by other main stream nanotube separation methods, especially the density gradient ultracentrifugation (DGU) method. To carry out this comparison, we first compared the optical absorption spectra of semiconducting arc-discharge nanotubes

separated by DGU (blue curve) and gel-based column chromatographic (red curve) methods, which are shown in Figure 4a. Here we chose 99% separated semiconducting nanotubes purchased from Nanointegris Inc. as the reference DGU-based separated nanotube sample. From this plot, one can find that very similar optical absorption spectra were obtained for DGU-based and gel-based separated

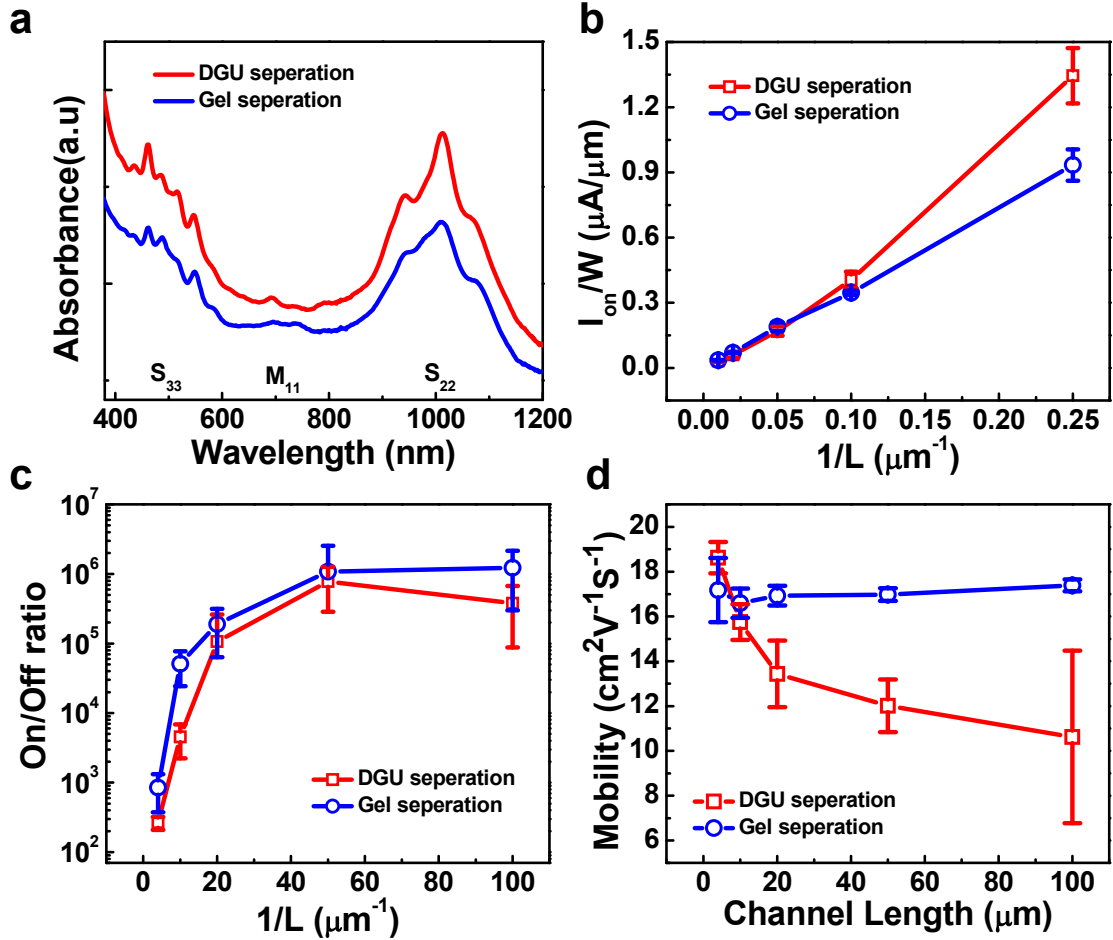


Figure 5. Comparison of key device performance metrics of SN-TFTs using semiconducting arc-discharge nanotubes separated by DGU and gel-based column chromatographic methods. (a) Optical absorption spectra of semiconducting arc-discharge nanotubes separated by DGU (blue) and gel-based column chromatographic (red) methods. (b) Current density ( $I_{on}/W$ ) versus reversed channel length for TFTs fabricated on semiconducting nanotubes separated by DGU (blue) and gel-based (red) methods. Plot of (b) average on/off ratio ( $I_{on}/I_{off}$ ) and (c) device mobility ( $\mu_{device}$ ) versus channel length for the same devices measured in (b).

nanotubes, which suggests that these two kinds of nanotubes share similar purity as well as diameter distribution. Starting with these two kinds of semiconducting nanotubes, we have fabricated 120 SN-TFTs (each kind of nanotubes have 60 SN-TFTs) and compared their performance. Figure 5b-d summarize the statistic key parameters of the DGU-based and gel-based arc-discharge SN-TFTs. The on-current density and on/off ratio information can be found in Figure 5b and d, which reveal that DGU-based separated SN-TFTs provide slightly higher on-current density but lower on/off ratio than gel-based SN-TFTs. This behaviour may due to the fact that DGU-separated nanotubes have longer average length (~1  $\mu\text{m}$ ) than gel-based arc-discharge nanotubes (540 nm) leading to fewer nanotube-to-nanotube junctions and therefore lower sheet resistance, but higher probability of metallic nanotube pass for DGU-separated nanotubes. Besides on-current and on/off ratio, device mobility is also studied in Figure 4d. Based on this figure, one can find that gel-based arc-discharge SN-TFTs show slightly higher mobility than DGU-based SN-TFTs when the channel length is longer than 20  $\mu\text{m}$ . Overall, although there are some small differences between gel-based and DGU-based arc-discharge SN-TFTs, these two kinds of devices provide similar electrical performance, which suggests that in terms of electrical property, gel-based separated semiconducting nanotubes are comparable to DGU separated semiconducting nanotubes.

## Conclusion

In conclusion, we report our progress on gel-based column chromatographic nanotube separation of different kinds of nanotubes and its application in macroelectronics, including progress on the detailed analysis of key performance metrics of devices using gel-based arc-discharge, HiPCO and CoMoCAT semiconducting nanotubes, and direct

comparison of the electrical property of gel-based and DGU-based separated semiconducting nanotubes. We have revealed the trade-off between transistor mobility and on/off ratio depending on the nanotube diameter. While large-diameter nanotubes (arc-discharge) lead to high device mobility, small-diameter nanotubes (HiPCO and CoMoCAT) can provide high on/off ratio ( $>10^6$ ) for transistors with comparable dimensions. In addition, based on our analysis, gel-based SN-TFTs have satisfied the requirement of large scale AMOLED high definition displays and can be a promising candidate of the transistors used in next generation displays. Moreover, we have pointed out that due to the trade-off between on-current density and on/off ratio for SN-TFTs, instead of mobility, maximum on-current density for devices with on/off ratio above certain threshold should be the main parameter to evaluate the electrical performance of carbon nanotube thin-film transistors. Furthermore, we have carried out the comparison between gel-based and DGU-based separated nanotubes, and found that both methods can provide separated nanotubes with similar electrical performance. Our work represents significant advance in the gel-based separated nanotube thin-film electronics, and may provide guide to future research on SN-TFT based macroelectronics.

## Methods

**Carbon nanotube dispersion:** Arc-discharge nanotubes were dispersed in water with the assistant of sodium cholate (SC) with a concentration of 1 mg/mL, while HiPCO and CoMoCAT nanotubes were dispersed in aqueous solution assisted by 1% sodium dodecyl sulfate (SDS, Sigma-Aldrich (99%)) at 0.3 mg/ml and 1 mg/mL, respectively. All three kinds of nanotubes were sonicated using a tip-type ultrasonic homogenizer (Sonicator 3000, Misonix) for 2 hours at 9 Watts in a water/ice bath. After sonication, the solution was centrifuged to

remove any possible bundles or impurities (20,000 rpm for 3 hour at 14 °C). The resulting supernatant was collected as Arc-discharge, HiPCO and CoMoCAT SWNT solutions.

**Nanotube separation by gel-based column chromatography.** First, sephacryl medium (GE healthcare, Inc.) was filled into a typical column (30 cm in length and 2 cm in width). Second, the column was equilibrated by flushing with 1% SDS solution. The nanotube solution was then added to the column. After that 1% SDS solution was used to elute the column, and metallic nanotubes were sorted out during this elution step. Following that, for arc-discharge and HiPCO nanotubes, 1% SC solution was added into the column to wash out the remaining semiconducting nanotubes, while 1% SDS+0.04% SC solution was used to get semiconducting CoMoCAT nanotubes.

**Separated Nanotube Deposition.** Aminopropyltriethoxy silane (APTES) was used to functionalize the Si/SiO<sub>2</sub> surface to form amine-terminated monolayer. This was done by immersing the Si/SiO<sub>2</sub> substrates into diluted APTES solution (1% APTES in isopropanol alcohol (IPA)) for 10 minutes. The samples were then rinsed with IPA, blew dry thoroughly and then immersed into separated nanotube solution for 30 minutes, after which uniform nanotube networks were formed on top of substrates.

**Back-Gated SN-TFT Fabrication.** 50 nm SiO<sub>2</sub> was used to act as the back-gate dielectric. The source and drain electrodes were patterned by photo-lithography, and 1nm Ti and 50 nm Pd are deposited followed by the lift-off process to form the source and drain metal contacts. Finally, since the separated nanotube thin film cover the entire wafer, in order to achieve accurate channel length and width, and to remove the possible leakage in the devices, one more step of photo-lithography plus O<sub>2</sub> plasma was used to remove the unwanted

nanotubes outside the device channel regions.

*Acknowledgment.* We acknowledge financial support from University of Southern California. We thank Dr. Ming Zheng of National Institute of Standards and Technology for valuable discussions.

**Electronic Supplementary Material:** Raman of arc-discharge, HiPCO and CoMoCAT semiconducting nanotubes (S1); Purity and diameter calculation of gel-based separated nanotubes (S2); Off-current *versus* channel length for three kinds of SN-TFTs (S3). This material is available free of charge *via* the Internet at [http://dx.doi.org/10.1007/s12274-\\*\\*\\*-\\*\\*\\*\\*-](http://dx.doi.org/10.1007/s12274-***-****-)

## References

1. Iijima, S. Helical Microtubules of Graphitic Carbon. *Nature* **1991**, 354, 56-58.
2. Bockrath, M.; Cobden, D. H.; McEuen, P. L.; Chopra, N. G.; Zettl, A.; Thess, A.; Smalley, R. E. Single-Electron Transport in Ropes of Carbon Nanotubes. *Science* **1997**, 275, 1922-1925.
3. Odom, T. W.; Huang, J. L.; Kim, P.; Lieber, C. M. Atomic Structure and Electronic Properties of Single-Walled Carbon Nanotubes. *Nature* **1998**, 391, 62-64.
4. Wildoer, J. W. G.; Venema, L. C.; Rinzler, A. G.; Smalley, R. E.; Dekker, C. Electronic Structure of Atomically Resolved Carbon Nanotubes. *Nature* **1998**, 391, 59-62.
5. Bachtold, A.; Hadley, P.; Nakanishi, T.; Dekker, C. Logic Circuits with Carbon Nanotube Transistors. *Science* **2001**, 294, 1317-1320.
6. Javey, A.; Guo, J.; Wang, Q.; Lundstrom, M.; Dai, H. J. Ballistic Carbon Nanotube Field-Effect Transistors. *Nature* **2003**, 424, 654-657.
7. Chen, Z.; Appenzeller, J.; Lin, Y.-M.; Sippel-Oakley, J.; Rinzler, A. G.; Tang, J.; Wind, S. J.; Solomon, P. M.; Avouris, P. An Integrated Logic Circuit Assembled on a Single Carbon Nanotube. *Science* **2006**, 311, 1735.
8. Liu, X. L.; Lee, C.; Zhou, C. W.; Han, J. Carbon Nanotube Field-Effect Inverters. *Appl. Phys. Lett.* **2001**, 79, 3329-3331.
9. Ryu, K.; Badmaev, A.; Wang, C.; Lin, A.; Patil, N.; Gomez, L.; Kumar, A.; Mitra, S.; Wong, H. S.; Zhou, C. Cmos-Analogous Wafer-Scale Nanotube-on-Insulator Approach for Submicrometer Devices and Integrated Circuits Using Aligned Nanotubes. *Nano Lett.* **2009**, 9, 189-97.

10. Kang, S. J.; Kocabas, C.; Ozel, T.; Shim, M.; Pimparkar, N.; Alam, M. A.; Rotkin, S. V.; Rogers, J. A. High-Performance Electronics Using Dense, Perfectly Aligned Arrays of Single-Walled Carbon Nanotubes. *Nat. Nanotechnol.* **2007**, *2*, 230-6.
11. Ding, L.; Zhang, Z. Y.; Liang, S. B.; Pei, T.; Wang, S.; Li, Y.; Zhou, W. W.; Liu, J.; Peng, L. M. Cmos-Based Carbon Nanotube Pass-Transistor Logic Integrated Circuits. *Nature communications* **2012**, *3*.
12. Franklin, A. D.; Chen, Z. H. Length Scaling of Carbon Nanotube Transistors. *Nat. Nanotechnol.* **2010**, *5*, 858-862.
13. Wang, C.; Zhang, J.; Ryu, K. M.; Badmaev, A.; De Arco, L. G.; Zhou, C. Wafer-Scale Fabrication of Separated Carbon Nanotube Thin-Film Transistors for Display Applications. *Nano Lett.* **2009**, *9*, 4285-4291.
14. Snell, A. J.; Mackenzie, K. D.; Spear, W. E.; Lecomber, P. G.; Hughes, A. J. Application of Amorphous-Silicon Field-Effect Transistors in Addressable Liquid-Crystal Display Panels. *Appl. Phys.* **1981**, *24*, 357-362.
15. Forrest, S. R. The Path to Ubiquitous and Low-Cost Organic Electronic Appliances on Plastic. *Nature* **2004**, *428*, 911-918.
16. Gelinck, G. H.; Huitema, H. E.; van Veenendaal, E.; Cantatore, E.; Schrijnemakers, L.; van der Putten, J. B.; Geuns, T. C.; Beenhakkers, M.; Giesbers, J. B.; Huisman, B. H.; *et al.* Flexible Active-Matrix Displays and Shift Registers Based on Solution-Processed Organic Transistors. *Nat. Mater.* **2004**, *3*, 106-10.
17. Klauk, H.; Halik, M.; Zschieschang, U.; Eder, F.; Rohde, D.; Schmid, G.; Dehm, C. Flexible Organic Complementary Circuits. *IEEE Trans. Electron Devices* **2005**, *52*, 618-622.
18. Uchikoga, S. Low-Temperature Polycrystalline Silicon Thin-Film Transistor Technologies for System-on-Glass Displays. *Mrs. Bull.* **2002**, *27*, 881-886.
19. Chang, C. P.; Wu, Y. S. Improved Electrical Performance of Milc Poly-Si Tfts Using Cf4 Plasma by Etching Surface of Channel. *Ieee. Electr. Device. L* **2009**, *30*, 130-132.
20. Nomura, K.; Ohta, H.; Ueda, K.; Kamiya, T.; Hirano, M.; Hosono, H. Thin-Film Transistor Fabricated in Single-Crystalline Transparent Oxide Semiconductor. *Science* **2003**, *300*, 1269-1272.
21. Nomura, K.; Ohta, H.; Takagi, A.; Kamiya, T.; Hirano, M.; Hosono, H. Room-Temperature Fabrication of Transparent Flexible Thin-Film Transistors Using Amorphous Oxide Semiconductors. *Nature* **2004**, *432*, 488-492.
22. Arnold, M. S.; Stupp, S. I.; Hersam, M. C. Enrichment of Single-Walled Carbon Nanotubes by Diameter in Density Gradients. *Nano Lett.* **2005**, *5*, 713-718.
23. Arnold, M. S.; Green, A. A.; Hulvat, J. F.; Stupp, S. I.; Hersam, M. C. Sorting Carbon Nanotubes by Electronic Structure Using Density Differentiation. *Nat. Nanotechnol.* **2006**, *1*, 60-5.
24. Engel, M.; Small, J. P.; Steiner, M.; Freitag, M.; Green, A. A.; Hersam, M. C.; Avouris, P. Thin Film Nanotube Transistors Based on Self-Assembled, Aligned, Semiconducting Carbon Nanotube Arrays. *ACS Nano* **2008**, *2*, 2445-52.
25. Sangwan, V. K.; Ortiz, R. P.; Alaboson, J. M. P.; Emery, J. D.; Bedzyk, M. J.; Lauhon, L. J.; Marks, T. J.; Hersam, M. C. Fundamental Performance Limits of Carbon Nanotube Thin-Film Transistors Achieved Using Hybrid Molecular Dielectrics. *ACS Nano* **2012**, *6*, 7480-7488.
26. Wang, C.; Zhang, J.; Zhou, C. Macroelectronic Integrated Circuits Using High-Performance Separated Carbon Nanotube Thin-Film Transistors. *ACS Nano* **2010**, *4*, 7123-7132.
27. Zhang, J.; Wang, C.; Fu, Y.; He, Y. C.; Zhou, C. Air-Stable Conversion of Separated Carbon Nanotube Thin-Film Transistors from p-Type to n-Type Using Atomic Layer Deposition of High-Kappa Oxide and Its Application in Cmos Logic Circuits. *ACS Nano* **2011**, *5*, 3284-3292.
28. Zhang, J.; Wang, C.; Zhou, C. Rigid/Flexible Transparent Electronics Based on Separated Carbon Nanotube Thin-Film Transistors and Their Application in Display Electronics. *ACS Nano* **2012**, *6*, 7412-7419.
29. Zhang, J.; Fu, Y.; Wang, C.; Chen, P. C.; Liu, Z. W.; Wei, W.; Wu, C.; Thompson, M. E.; Zhou, C. Separated Carbon Nanotube Macroelectronics for Active Matrix Organic Light-Emitting Diode Displays. *Nano Lett.* **2011**, *11*, 4852-4858.
30. Tanaka, T.; Jin, H.; Miyata, Y.; Fujii, S.; Suga, H.; Naitoh, Y.; Minari, T.; Miyadera, T.; Tsukagoshi, K.; Kataura, H. Simple and Scalable Gel-Based Separation of Metallic and Semiconducting Carbon Nanotubes. *Nano Lett.* **2009**, *9*, 1497-1500.
31. Moshhammer, K.; Hennrich, F.; Kappes, M. M. Selective Suspension in Aqueous Sodium Dodecyl Sulfate According to Electronic Structure Type Allows Simple Separation of Metallic from Semiconducting Single-Walled Carbon Nanotubes. *Nano Research* **2009**, *2*, 599-606.
32. Liu, H. P.; Nishide, D.; Tanaka, T.; Kataura, H. Large-Scale Single-Chirality Separation of Single-Wall Carbon Nanotubes by Simple Gel Chromatography. *Nature communications* **2011**, *2*.
33. Gui, H.; Li, H. B.; Tan, F. R.; Jin, H. H.; Zhang, J.; Li, Q. W. Binary Gradient Elution of Semiconducting Single-Walled Carbon Nanotubes by Gel Chromatography for Their Separation According to Chirality. *Carbon* **2012**, *50*, 332-335.
34. Miyata, Y.; Shiozawa, K.; Asada, Y.; Ohno, Y.; Kitaura, R.; Mizutani, T.; Shinohara, H. Length-Sorted Semiconducting Carbon Nanotubes for High-Mobility Thin Film Transistors. *Nano Research* **2011**, *4*, 963-970.
35. Miyata, Y.; Yanagi, K.; Maniwa, Y.; Kataura, H. Optical Evaluation of the Metal-to-Semiconductor Ratio of Single-Wall Carbon Nanotubes. *J. Phys. Chem. C* **2008**, *112*, 13187-13191.
36. Nirmalraj, P. N.; Lyons, P. E.; De, S.; Coleman, J. N.; Boland, J. J. Electrical Connectivity in Single-Walled Carbon Nanotube Networks. *Nano Lett.* **2009**, *9*, 3890-5.

37. Asada, Y.; Nihey, F.; Ohmori, S.; Shinohara, H.; Saito, T. Diameter-Dependent Performance of Single-Walled Carbon Nanotube Thin-Film Transistors. *Adv. Mater.* **2011**, *23*, 4631-5.
38. Pike, G. E.; Seager, C. H. Percolation and Conductivity: A Computer Study. I. *Phys. Rev. B* **1974**, *10*, 1421-1434.
39. Kwon, O.-K. TFT Mobility Requirement for AMOLED Hdtvs. *Thin film transistor technologies (TFTT VII) : proceedings of the international symposium* **2004**, 146.
40. Gu, G.; Forrest, S. R. Design of Flat-Panel Displays Based on Organic Light-Emitting Devices. *Ieee. J. Sel. Top. Quant* **1998**, *4*, 83-99.
41. Kang, S. J.; Kocabas, C.; Ozel, T.; Shim, M.; Pimparkar, N.; Alam, M. A.; Rotkin, S. V.; Rogers, J. A. High-Performance Electronics Using Dense, Perfectly Aligned Arrays of Single-Walled Carbon Nanotubes. *Nature Nanotechnol.* **2007**, *2*, 230-236.
42. Cao, Q.; Xia, M.; Kocabas, C.; Shim, M.; Rogers, J. A.; Rotkin, S. V. Gate Capacitance Coupling of Singled-Walled Carbon Nanotube Thin-Film Transistors. *Appl. Phys. Lett.* **2007**, *90*, 023516-1-3.
43. Rosenblatt, S.; Yaish, Y.; Park, J.; Gore, J.; Sazonova, V.; McEuen, P. L. High Performance Electrolyte Gated Carbon Nanotube Transistors. *Nano Lett.* **2002**, *2*, 869-872